Synthesis, phase diagram and magnetic properties of $(1 − x)$BiFeO$_3$−xLaMnO$_3$ Solid Solution

CrossMark

Jiangtao Wu [a,b,*], Nan Li [a], Jun Xu [a], Shuang Zhou [a], Yaqi Jiang [a], Zhaoxiong Xie [a,*]

[a] State Key Laboratory of Physical Chemistry of Solid Surface & Department of Chemistry, College of Chemistry and Chemical Engineering, Xiamen University, Xiamen 361005, China
[b] College of Chemistry and Materials Science, Sichuan Normal University, Chengdu 610068, China

A B S T R A C T

In this paper, we report the syntheses of $(1 − x)$BiFeO$_3$–xLaMnO$_3$ solid solution ($x = 0$–1) by an improved sol–gel method. With careful characterization of crystal structures of the as-prepared products and the phase transition as a function of temperature, the phase diagram of $(1 − x)$BiFeO$_3$–xLaMnO$_3$ solid solution has been determined. With the increasing of x value, the crystal structure of the samples transforms from rhombohedral $R3c$ ($x \leqslant 0.13$) to tetragonal $P4mm$ ($0.14 \leqslant x \leqslant 0.25$), cubic $Pm\bar{3}m$ ($0.26 \leqslant x \leqslant 0.78$), and finally to rhombohedral $R\bar{3}c$ ($0.80 \leqslant x \leqslant 1.00$). In situ high temperature X-ray powder diffraction (HTXRD) studies reveal that the phase transformations of rhombohedral $R3c$ to orthorhombic $Pbnm$ and tetragonal $P4mm$ to orthorhombic $Pbnm$ occur at 600–750 °C and 580–700 °C, respectively. The phase structures of cubic $Pm\bar{3}m$ and rhombohedral $R\bar{3}c$ keep unchanged at temperature below 880 °C. However, a second-order-like phase transition was observed at higher temperature because of the change of thermo expansion coefficient. The complete phase diagram was then drawn based on those experimental results. It can be found clearly from the phase diagram that the as-prepared $(1 − x)$BiFeO$_3$–xLaMnO$_3$ ($x = 0$–1) solid solutions provided more options to tune the magnetism and multiferroism, as the crystal structures possess polarity feature at a wide doping concentration of LaMnO$_3$ ($x \leqslant 0.25$). We then selectively studied the magnetic properties of possible multiferroic phases, i.e. $R3c$ and $P4mm$ phases. The results revealed that the magnetic property can be greatly enhanced when doping fraction of LaMnO$_3$ is more than 0.08 ($x > 0.08$).

© 2015 Elsevier B.V. All rights reserved.

1. Introduction

Multiferroic materials, showing the coexistence of ferroelectric and magnetic orders [1], have recently attracted intensive research interest due to fascinating fundamental physics and potential applications for new devices such as multiple-state memory elements, magnetic field sensors and magnetically modulated piezoelectric transducers [2–6]. Unfortunately, the incompatibility between ferroelectricity and ferromagnetism limits our choice of multiferroics, nature or synthesized single-phase high performance multiferroics are rare [7]. Bismuth ferrite, BiFeO$_3$ (abbreviated as BFO) is one of the few single-phase multiferroic materials at room temperature. Bulk BFO crystallizes in a rhombohedrally distorted perovskite structure [8], which space group is $R3c$, and lattice parameters are $a = b = c = 5.634$ Å and $\alpha = \beta = \gamma = 59.4°$. Its ferroelectricity property results from the shifts of Bi and Fe atoms,

and its Curie temperature T_C at 1103 K [9]. The magnetic moments between each Fe^{3+} ion and six nearest Fe^{3+} ions are antiparallel, resulting in G-type antiferromagnetism (Néel temperature $T_N = 643$ K) [10]. This structure permits a canting of antiferromagnetic sublattice. However, the weak ferromagnetic moments are canceled out by superimposed spiral spin structure with a period of 62 nm [11]. This unique structure greatly restricts the application of BFO due to lack of net spontaneous magnetization and linear magnetoelectric effect [12].

To enhance magnetic properties, physical and chemical modifications of BFO were usually carried out. For physical modification, causing crystal defects, and controlling particle size or thickness of a thin-film in nanometer scale can regulate the magnetism of BFO [13]. For example, introducing point defects of oxygen vacancies into BFO powders produced the ferromagnetism via a self-catalyzed fast reaction synthetic process [14]. Besides, chemical substitution is found to be an effective strategy to enhance the magnetic property of bulk BFO. For example, chemically modified multiferroic $(1 − x)$BiFeO$_3$–xDyFeO$_3$ solid solution exhibited an enhanced magnetization [15,16]. It is generally accepted that the magnetic properties of ferrites depend on magnetic interactions,

* Corresponding authors at: College of Chemistry and Materials Science, Sichuan Normal University, Chengdu 610068, China (J. Wu). Tel.: +86 592 2180627, +86 18328745878; fax: +86 592 2183047.
E-mail addresses: jtwu@sicnu.edu.cn (J. Wu), zxxie@xmu.edu.cn (Z. Xie).

which can be modified by substitution of Bi^{3+} and Fe^{3+} ions by other elements. Substituting Bi^{3+} with rare earth elements, which have similar radius to that of Bi^{3+}, may enhance the magnetic property and prevent the impurity in the synthesis process [17–19]. Substituting Fe^{3+} with transition metal elements can suppress the spiral spin structure and lead to weak ferromagnetic property [20–22]. Recently, co-substitutions of Bi^{3+} and Fe^{3+} ions were also studied. Solid solution of $LaMnO_3$–$BiFeO_3$ (co-substitution of Bi^{3+} and Fe^{3+} ions with La^{3+} and Mn^{3+} ions respectively) is a good model system for co-substitution, because $BiFeO_3$ and $LaMnO_3$ possess the similar perovskite structure and ionic radii, which helps form homogeneous solid solution. Although the radius of La^{3+} ion (0.116 nm) and Bi^{3+} ion (0.117 nm) are almost same, their physical and chemical properties are much different, which help to tune multiferroic properties. Lahmar et al. reported the synthesis and electric property of $LaMnO_3$–$BiFeO_3$ thin film solid solution (the composition of $LaMnO_3$ less than 10%) [23,24]. To date, there is no systematic exploration on $(1 - x)BiFeO_3$–$xLaMnO_3$ solid solution and its complete phase diagram. It is well known that the crystal structure could transform with the increasing amount of substituting elements, and is critical for the multiferroic properties of samples. Therefore, it is important to investigate the phase transition and the properties with respect to the doping concentration. In this study, we systematically investigated the structure and magnetic properties of $(1 - x)BiFeO_3$–$xLaMnO_3$ solid solution to further explorer the intrinsic multiferroic properties. A series of binary solid solutions of $(1 - x)BiFeO_3$–$xLaMnO_3$ ($x = 0$–1) were synthesized by improved sol–gel method and detailed phase diagram of this binary solid solution was constructed. According to the phase diagram, we selectively studied the magnetic properties of possible multiferroic phases, i.e. $R3c$ and $P4mm$ phases. It was found the solid solutions exhibit greatly enhanced magnetization at 2 K when $x > 0.8$ and the co-substitution of La^{3+} and Mn^{3+} for Bi^{3+} and Fe^{3+} can enhance ferromagnetism while retaining the ferroelectricity of BFO.

2. Experimental

2.1. Synthesis of $(1 - x)BiFeO_3$–$xLaMnO_3$ ($x = 0$–1) powders

$(1 - x)BiFeO_3$–$xLaMnO_3$ ($x = 0$–1) powders were prepared by two-step process. Firstly, the stoichiometric mixtures of analytical-grade purity $Mn(NO_3)_2$ (50%), $La(NO_3)_3 \cdot 6H_2O$, $Fe(NO_3)_3 \cdot 9H_2O$ and $Bi(NO_3)_3 \cdot 5H_2O$ were homogenized in dilute nitric acid. Then, tartaric acid was added in the resulting solution, the molar ratio of tartaric acid with metal ions was 5:1. The solution was heated in heating jacket (250 °C) until powders appeared. Secondly, the powders were calcined at 850 °C for 3 h in the furnace.

2.2. Characterization of $(1 - x)BiFeO_3$–$xLaMnO_3$ ($x = 0$–1) powders

X-ray powder diffraction (XRD) experiments were performed using a PANalytical X'pert diffractometer with Cu Kα radiation (X'pert PRO, PANalytical B.V.). The data were taken with a step size of 0.016° and a step time of 10 s, operating at 30 mA and 40 kV. For in-situ high temperature X-ray diffraction (HTXRD) measurements, $(1 - x)BiFeO_3$–$xLaMnO_3$ powders were subjected to high temperature XRD attachment and the HTXRD patterns were collected in air on the PANalytical X'pert PRO diffractometer. The temperature range is from 25 °C to 880 °C. A heating rate of 10 K/min and a soaking time of 10 min were employed. The Rietveld refinement was carried out using X'Pert Highscore Plus software. Magnetic measurements were performed using a Superconducting Quantum Interference Device (SQUID, MPMS-XL-7, Quantum Design Inc., USA).

3. Results and discussion

3.1. The composition-driven phase transition of $(1 - x)BiFeO_3$–$xLaMnO_3$ ($x = 0$–1)

In order to investigate the complete phase diagram of $(1 - x)BiFeO_3$–$xLaMnO_3$ ($x = 0$–1) at room temperature, we studied X-ray powder diffraction of $(1 - x)BiFeO_3$–$xLaMnO_3$ ($x = 0$–1)

samples. As shown in Fig. 1a, when $x \leqslant 0.13$, the diffractions can be indexed to a rhombohedral structure ($R3c$); tetragonal phase ($P4mm$) appears when $0.14 \leqslant x \leqslant 0.25$; the structure of samples changes to a cubic phase ($Pm\bar{3}m$) when $0.26 \leqslant x \leqslant 0.78$; when $0.80 \leqslant x \leqslant 1.00$, the structure transforms to rhombohedral phase with space group of $R\bar{3}c$. Even though the XRD diffraction patterns of all as-prepared samples are similar at a brief glance, it can be found subtle differences in some typical diffraction peak profiles with a carful observation. The enlarged XRD patterns were shown in Fig. 1b. When $x = 0.13$, the sample adopts the same crystal structure of BFO, which belongs to rhombohedral phase with a space group of $R3c$. For this phase, the diffraction at 22.5° appears in one peak, which corresponds to (012) diffraction; and the diffraction around 32° consists of two peaks, corresponding to (104) and (110) diffractions. When x value increases to 0.14, the diffractions at 22.5° and 46° split into two peaks, corresponding to (001), (100) and (002), (200) diffractions, respectively, which are characteristic peaks of tetragonal phase with a space group $P4mm$. The structure of these samples is an isomorphism of $BaTiO_3$. When the x value further increases to 0.26, the diffraction at about 22.5° changes again to a single peak (corresponding to (100) diffraction). In addition, the diffractions at about 32° and 46° also change to single peaks. Such results indicate the crystal structure of solid solution has transformed to higher symmetry and a cubic phase with the space group of $Pm\bar{3}m$ is determined. Interestingly, when x value further increases to 0.80, two diffraction peaks (i.e. (110) and (104)) at about 32° appear again, indicating the crystal symmetry decreases to a rhombohedral lattice ($R\bar{3}c$), which is the typical phase of bulk $LaMnO_3$. The driving force of phase transition is the difference of chemistry properties of La^{3+} and Mn^{3+} ions.

To further confirm the relationship of phase transition of $(1 - x)BiFeO_3$–$xLaMnO_3$ ($x = 0$–1) and the composition, the XRD data at room temperature were refined by Rietveld refinement using X'pert Highscore Plus software. We respectively adopted atomic coordinates from $BiFeO_3$ type-$R3c$, $BaTiO_3$ type-$P4mm$, $LaMnO_3$ type-$Pm\bar{3}m$ and $LaMnO_3$ type-$R\bar{3}c$ as the original atomic coordinates to refine the structure with corresponding phases. The refinement results were listed in Table 1. Fig. 2 shows the observed (dotted line) and calculated (continuous line) XRD patterns, and the deviations (bottom line) for $(1 - x)BiFeO_3$–$xLaMnO_3$ ($x = 0.10$, 0.20, 0.40, 0.90). The R_P/R_{WP} for $x = 0.10$, 0.20, 0.40 and 0.90 are 5.43/7.35, 7.08/9.08, 6.92/9.30 and 5.33/7.06, respectively. It can be found that all the calculated data fit well with the observed data, which further confirms our phase determination is correct.

The rhombohedral structure ($R3c$) of pure BFO can be considered as a distortion from an ideal cubic perovskite $Pm\bar{3}m$ structure [25]. There exist two steps of distortion in the structure evolution from $Pm\bar{3}m$ to $R3c$. One is the ferroelectric distortion along [111] direction, evolving from $Pm\bar{3}m$ to $R3m$ [25]. Crystal with $R3m$ space group shows ferroelectric property, whereas does not show ferromagnetism. The other is a relative rotation of two oxygen octahedra in the opposite direction around [111] direction, leading to the evolution from $Pm\bar{3}m$ to $R\bar{3}c$. Crystal with $R\bar{3}c$ shows weak ferromagnetism, whereas does not show ferroelectric property. When above-mentioned two distortions occur simultaneously, the crystal structure of $Pm\bar{3}m$ turns to be $R3c$, and it will show both ferroelectric and weak ferromagnetic properties [25]. From the crystal model of $(1 - x)BiFeO_3$–$xLaMnO_3$ ($x = 0.10$, 0.20, 0.40, 0.90) samples shown in Fig. 2, we found that the ferroelectric distortion and the rotation of oxygen octahedra decrease with the increasing amount of $LaMnO_3$. When the amount of $LaMnO_3$ increases to 40% (i.e. $x = 0.40$), crystal structure of the product changes into cubic $Pm\bar{3}m$, in which both distortions disappeared and the
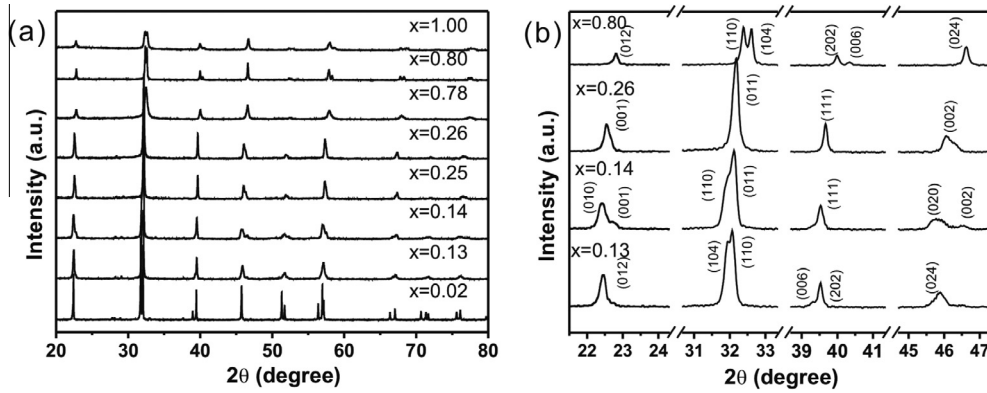
Fig. 1. (a) XRD patterns of $(1 - x)BiFeO_3 - xLaMnO_3$ (x = 0.02, 0.13, 0.14, 0.25, 0.26, 0.78, 0.80, 1.00) and (b) the magnified XRD patterns of $(1 - x)BiFeO_3 - xLaMnO_3$ (x = 0.13, 0.14, 0.26, 0.80) from 2θ = 20–47.5°.

Table 1
Refined structure parameters for $(1 - x)BiFeO_3 - xLaMnO_3$ (x = 0.10, 0.20, 0.40, 0.90).

Composition	Crystal structure	Lattice parameters (Å) and volume (Å³)	Atomic positions	Statistical parameter
0.1LaMnO₃–0.9BiFeO₃	Rhombohedral structure ($R3c$)	a = 5.5726(1) c = 13.7872(4) V = 370.79(2)	Bi/La(0,0,0) Fe/Mn(0,0,0.2243) O1(0.4373,0.0076,0.9573)	R_P = 5.43 R_{WP} = 7.35
0.2LaMnO₃–0.8BiFeO₃	Tetragonal structure ($P4mm$)	a = 3.9457(2) c = 3.9111(2) V = 61.10(1)	Bi/La(0,0,0) Fe/Mn(0.5,0.5,0.5135) O1(0.5,0.5,0.0531) O2(0.5,0,−0.4135)	R_P = 7.08 R_{WP} = 9.08
0.4LaMnO₃–0.6BiFeO₃	Cubic structure ($Pm\bar{3}m$)	a = 3.9172(2) V = 60.11(1)	Bi/La(0,0,0) Fe/Mn(0.5,0.5,0.5) O1(0.5,0.5,0)	R_P = 6.92 R_{WP} = 9.30
0.9LaMnO₃–0.1BiFeO₃	Rhombohedral structure ($R\bar{3}c$)	a = 5.5091(3) c = 13.3827(8) V = 351.25(3)	Bi/La(0,0,0.25) Fe/Mn(0,0,0) O1(0.5332,0,0.25)	R_P = 5.33 R_{WP} = 7.06
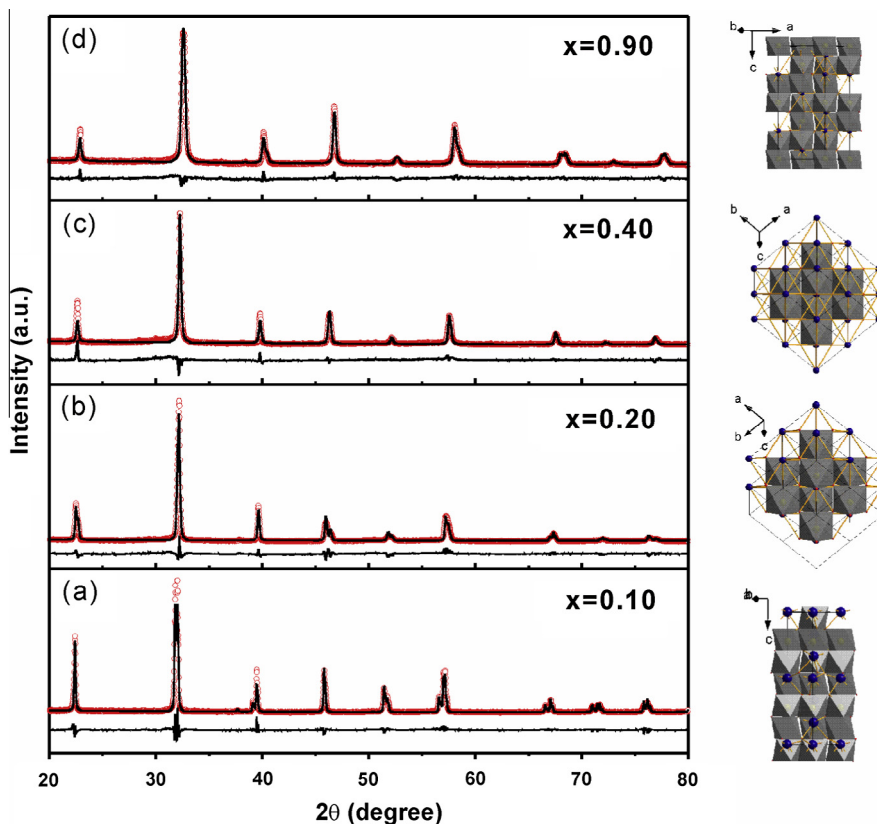
Fig. 2. Rietveld refinement of the XRD patterns for $(1 - x)BiFeO_3 - xLaMnO_3$ (a) x = 0.10 (BiFeO₃ type-$R3c$), (b) x = 0.20 (BaTiO₃ type-$P4mm$), (c) x = 0.40 (LaMnO₃ type-$Pm\bar{3}m$), (d) x = 0.90 (LaMnO₃ type-$R\bar{3}c$). The observed (dotted line), calculated (continuous line) XRD patterns, the deviations (bottom line) and crystal model are shown.
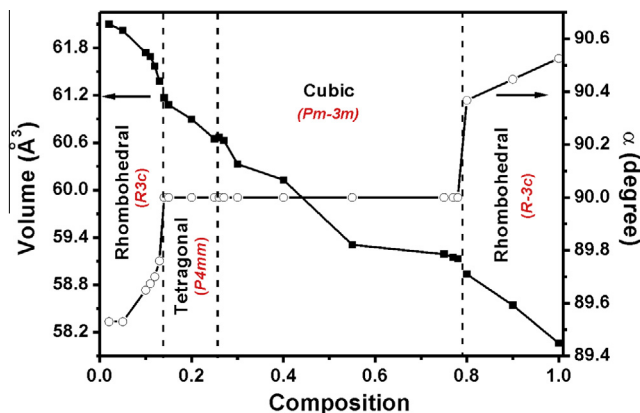
Fig. 3. Volumes per molecule and pseudo cell angles of basic perovskite unit of $(1 − x)BiFeO_3–xLaMnO_3$ (x = 0.02, 0.05, 0.10, 0.11, 0.12, 0.13, 0.14, 0.15, 0.20, 0.25, 0.26, 0.30, 0.40, 0.55, 0.70, 0.75, 0.80, 0.90, 1.00).

structure adopted an ideal cubic perovskite structure. When the value of x further increases, oxygen octahedra relatively rotate along [1 1 1] direction, resulting in the structure transforming from $Pm\bar{3}m$ to $R\bar{3}c$.

In order to easily analyze the crystal transition with the doping amount of LaMnO$_3$, the volume per molecule (v) was employed, which is relative to the crystal density. The volume per molecule is expressed as $v = V/Z$, where V represents the volume of a conventional unit cell, and Z represents the number of molecule per unit (for the $R3c$ and $R\bar{3}c$ phases Z = 6, for the $P4mm$ and $Pm\bar{3}m$ phases, Z = 1). The volume per molecule and pseudo crystal cell angles (corresponding to a basic perovskite crystal unit cell) are depicted in Fig. 3, and the detailed conventional unit cell parameters and the

crystal cell parameters per molecule of $(1 − x)BiFeO_3–xLaMnO_3$ (x = 0–1) were listed in Table S1 in the supporting information. From Fig. 3, it can be found that volumes per molecule decrease with the increase of doping amount of LaMnO$_3$. In addition, the basic units compress along the body diagonal direction (corresponding to [1 1 1] direction of perovskite unit cell), resulting in the increase of the pseudo crystal cell angles from 89.53° to 90.53°.

Polar crystal structure is the prerequisite for ferroelectricity and multiferroism. For doping the BFO solely with La, phase transition from rhombohedral structure (noncentric structure) to orthorhombic one (centric space group C222) occurs at 15% La doped BFO [26], while a phase transition from the noncentric structure to centric one occurred at 20% Mn^{3+} doped BFO [27]. The as-prepared $(1 − x)BiFeO_3–xLaMnO_3$ (x = 0–1) solid solution possess polar crystal structure when the concentration of LaMnO$_3$ is less than 25%, it provides us more options to tune the magnetism and multiferroism.

3.2. The temperature-driven phase transition of $(1 − x)BiFeO_3–xLaMnO_3$ (x = 0–1)

In order to investigate the phase transition of $(1 − x)$BiFeO$_3$–xLaMnO$_3$ (x = 0–1) as a function of temperature, in-situ high temperature X-ray powder diffraction was performed. For the sake of simplicity, we take the crystal volume per molecule of different phases as a function of temperature in $(1 − x)$BiFeO$_3$–xLaMnO$_3$ solid solution. Fig. 4a shows the rhombohedral structure ($R3c$, x = 0.10) keeps unchanged and the crystal volume per molecule linearly increases with the temperature increasing from room temperature to 650 °C. Interestingly, the crystal volume per molecule suddenly decreases from 62.75 Å^3 to 62.26 Å^3 when the temperature reached 650 °C. It demonstrates that phase transition from rhombohedral
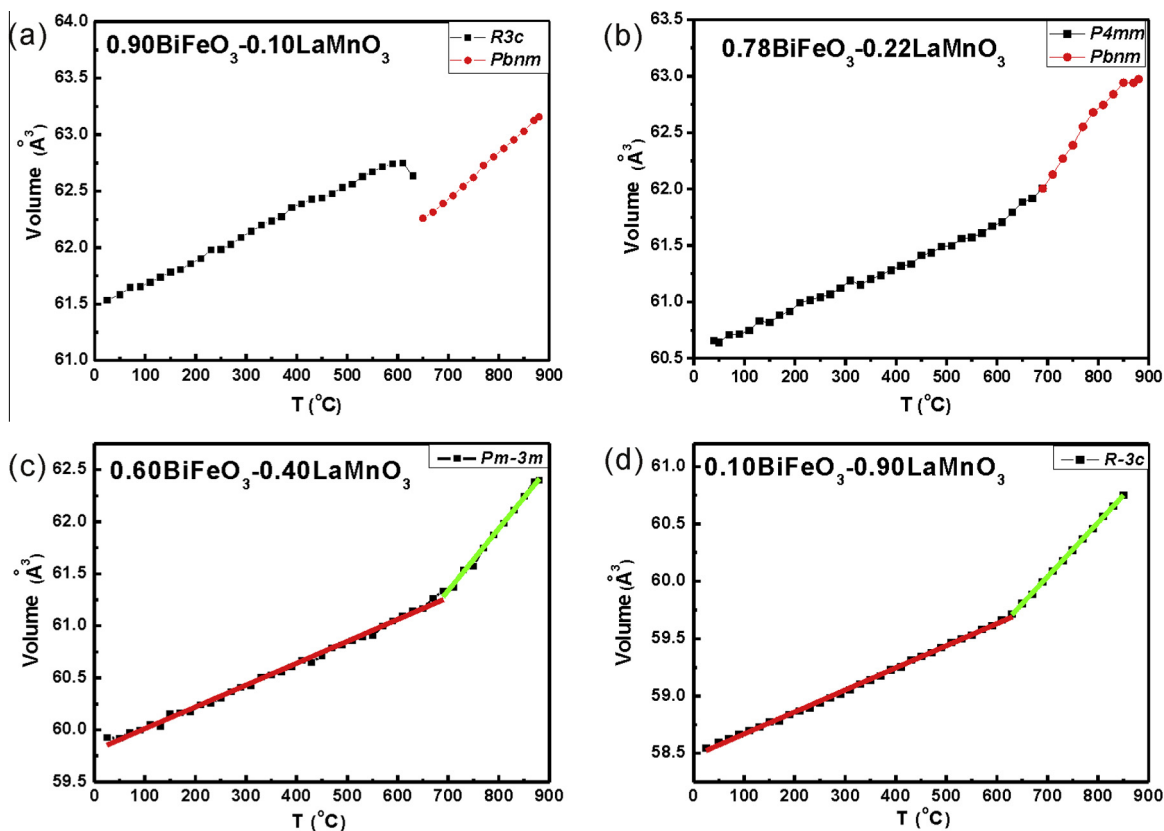
Fig. 4. Evolution of normalized unit cell volume of $(1 − x)BiFeO_3–xLaMnO_3$ as a function of temperature, (a) x = 0.10, (b) x = 0.22, (c) x = 0.40 and (d) x = 0.90.
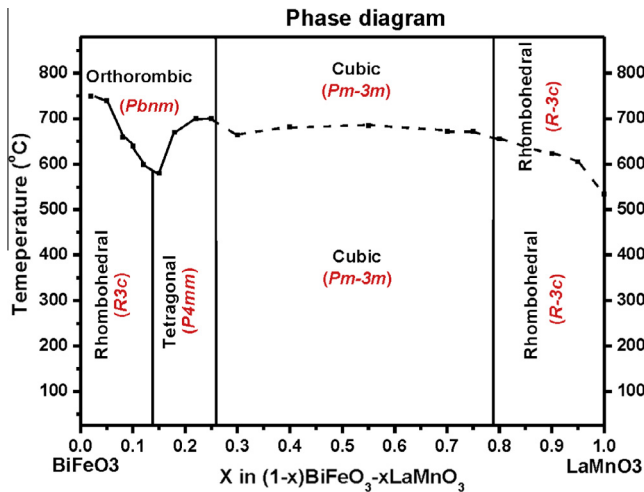
Fig. 5. Phase diagram of $(1 - x)BiFeO_3$–$xLaMnO_3$ system as a function of composition and temperature.

phase ($R3c$) to orthorhombic phase ($Pbnm$) occurs at 650 °C, which is also supported by the differential thermal analysis (see also Figs. S2 and S3 in the supporting information). This is corresponding to the first-order-like phase transition from ferroelectrics to paraelectrics [28]. From 650 °C to 880 °C, the cell volume per molecule of orthorhombic phase ($Pbnm$) increases linearly again. For the tetragonal phase ($P4mm$, $x = 0.22$), phase transition occurs at about 700 °C as shown in Fig. 4b, and orthorhombic phase ($Pbnm$) is determined when the temperature is above 700 °C. The differential thermal analysis suggests it could be also first-order phase transitions from $P4mm$ phase to $Pbnm$ phase (Fig. S4 in supporting information). For the cubic phase ($x = 0.40$), the structure of sample keeps

in cubic $Pm\bar{3}m$ phase in all temperature (Fig. 4c). However, there are two different tendencies of crystal cell volume as a function of temperature as shown by two straight lines (red and green lines) in Fig. 4c. The value of transition point is about 687 °C, which could suggest a second-order-like phase transition from ordered atoms to disorder atoms. Because the second order phase transition does not involves latent heat, the phase transition temperature cannot be determined by thermal analysis. Therefore, these phase transitions have been determined by cell parameters obtained from HTXRD refinement. Fig. 4d shows the case of rhombohedral $R\bar{3}c$ phase ($x = 0.90$). The structure of sample keeps in $R\bar{3}c$ phase, accompanying with a second-order-like phase transition at 624 °C.

3.3. Phase diagram of $(1 − x)BiFeO_3$–$xLaMnO_3$ $(x = 0–1)$

Combining the systematic results of XRD and HTXRD, the phase diagram for $(1 − x)BiFeO_3$–$xLaMnO_3$ $(x = 0–1)$ were drawn and shown in Fig. 5. The detailed phase transition temperatures were listed in Table S2 in the supporting information. At room temperature, crystal structures of $(1 − x)BiFeO_3$–$xLaMnO_3$ change from rhombohedral phase ($R3c$) to tetragonal phase ($P4mm$), cubic phase ($Pm\bar{3}m$) and finally rhombohedral phase ($R\bar{3}c$) with the increase of x value. When temperature increases, the rhombohedral phase ($R3c$) and tetragonal phase ($P4mm$) transform into the orthorhombic phase ($Pbnm$). The phase transition temperature of rhombohedral phase ($R3c$) decreases from 750 °C to 600 °C. The transition temperature of tetragonal phase ($P4mm$) increases from 580 °C to 700 °C. When $0.26 \leqslant x \leqslant 0.78$, it seems only cubic phases exist at temperature below 880 °C. However, based on the data of crystal cell volume as a function of temperature (Fig. 4c and d), we supposed that there could be a second-order-like phase transition from ordered atoms to disorder atoms at higher temperature. The phase of $LaMnO_3$, i.e. rhombohedral ($R\bar{3}c$) appears when $x \geqslant 0.80$.
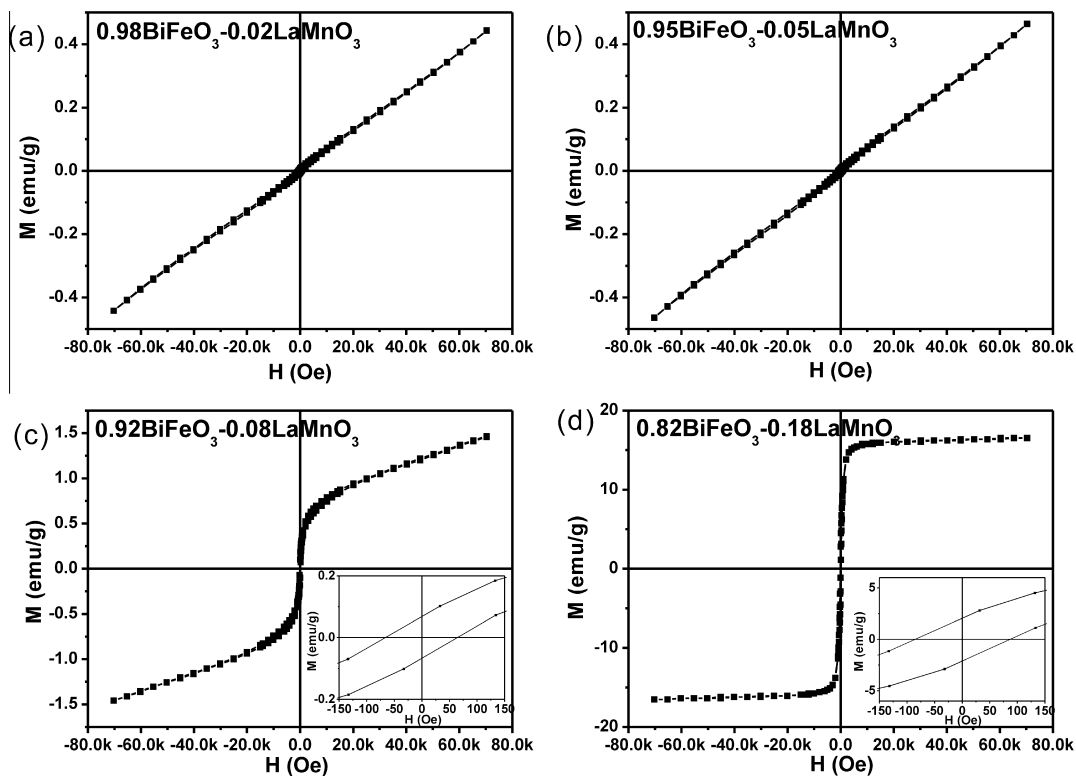
Fig. 6. Magnetization (M) versus field (H) curves for $(1 − x)BiFeO_3$–$xLaMnO_3$ solid solution ($x = 0.02, 0.05, 0.08, 0.18$) measured at 2 K. The insert is the magnified hysteresis loops. ($−150$ Oe $\leqslant H \leqslant 150$ Oe).

The structure of samples keeps rhombohedral $R\bar{3}c$ at temperature below 880 °C. However, there could be also a second-order-like phase transition at higher temperature according to the measurement of crystal cell volume as a function of temperature. The second-order-like phase transition temperature decreases from 656 °C to 535 °C when the x increases from 0.80 to 1.00.

3.4. Magnetic properties of $(1 − x)BiFeO_3–xLaMnO_3$ ($x = 0.02, 0.08, 0.20$)

Multiferroics requires both ferroelectric and ferromagnetism. By survey the phase diagram, it can be found that solid solutions with the rhombohedral ($R3c$) and tetragonal ($P4mm$) structures are significant because they are polar structure, and could be a good candidate of ferroelectric materials. Therefore, we studied the magnetic properties of the rhombohedral ($R3c$) and tetragonal ($P4mm$) phases. The hysteresis loops of $(1 − x)BiFeO_3–xLaMnO_3$ solid solutions ($x = 0.02, 0.05, 0.08, 0.18$) measured at 2 K were shown in Fig. 6. Obviously, the samples of $x = 0.02$ and $x = 0.05$ exhibit small magnetization and it varies lineally with respect to field strength, indicating they are typical antiferromagnetic materials. In contrast, when the doping amount of $LaMnO_3$ increases to 0.08, the magnetic hysteresis loop shows the M_S increases quickly at low external magnetic field (<1000 Oe) and it increases linearly at high magnetic field. Such a special hysteresis loop indicates the coexistence of antiferromegnetism and weak ferromagnetism, which is due to that La substitution partially breaks the spin cycloidal structure of the $BiFeO_3$-type structure. When x increases to 0.18, the hysteresis loop exhibits typical ferromagnetic property and the value of M_S sharply increases to 16.52 emu/g ($\sim$0.89 μ_B). As has been stated previously, La^{3+} ion is more likely to induce structure transition to turn off the ferroelectricity as well as suppress the spin cycloidal structure. In the present case, the La and Mn co-substitution induced a phase transition from $R3c$ to $P4mm$ structure when $x > 0.14$, and then the spin cycloid was destroyed and thus homogeneous magnetic structure was formed. Lin et al. reported the enhancement of ferromagnetic property via La doping (La content of 0.15) [26]. However, the magnetization value was very small (less than 1 emu/g), and the hysteresis loop was not saturated (almost liner), suggesting antiferromagnetism is dominated in the material. From our result, it can be found that the co-substitution of La and Mn can greatly increase the magnetization, because further substitution of Fe^{3+} ions with $Mn^{3+}(d^4)$ ions could break the balance between antiparallel sublattice magnetization due to John–Teller distortion of the MnO_6 coordination octahedron [23]. As a result, with appropriate substitution of La and Mn ions ($x < 0.25$), the magnetization of $(1 − x)BiFeO_3–xLaMnO_3$ solid solution can be greatly enhanced by destroy the cycloidal spiral antiferromagnetism, while keeping polar structures, which improves the multiferroic property of $BiFeO_3$.

4. Conclusions

In summary, we have studied the detailed phase transitions of $(1 − x)BiFeO_3–xLaMnO_3$ ($x = 0–1$) solid solutions as functions of compositions and temperature. The composition-driven phase transitions are rhombohedral $R3c$ ($x = 0–0.13$), tetragonal $P4mm$ ($x = 0.14–0.25$), cubic $Pm\bar{3}m$ ($x = 0.26–0.78$), and rhombohedral $R\bar{3}c$ ($x = 0.80–1.00$). The rhombohedral phase ($R3c$) and tetragonal phase ($P4mm$) transform into orthorhombic phase ($Pbnm$), with the increasing of temperature. The cubic phase ($Pm\bar{3}m$) and rhombohedral phase ($R\bar{3}c$) keep their structures until the temperature

reached 880 °C, but a second-order-like phase transition occurs. Combining the results of phase transition as functions of compositions and temperature, the phase diagram of $(1 − x)BiFeO_3–xLaMnO_3$ ($x = 0–1$) were constructed. According to the phase diagram, it can be found the as-prepared $(1 − x)BiFeO_3–xLaMnO_3$ ($x = 0–1$) solid solutions provide more options to tune the magnetism and multiferroism, as they are polar crystal structure at a wide doping concentration of $LaMnO_3$ (less than 25%). We further investigated the magnetic properties of the samples with the rhombohedral phase ($R3c$) and tetragonal phase ($P4mm$). The results reveals the solid solution $(1 − x)BiFeO_3–xLaMnO_3$ possesses enhanced magnetic property, and could be an ideal candidate for magnetoelectric application.

Appendix A. Supplementary material

Supplementary data associated with this article can be found, in the online version, at http://dx.doi.org/10.1016/j.jallcom.2015.01.283.

References

[1] H. Schmid, Ferroelectrics 162 (1994) 317.
[2] N.A. Spaldin, M. Fiebig, Science 309 (2005) 391.
[3] N.A. Hill, J. Phys. Chem. B 104 (2000) 6694.
[4] W. Eerenstein, N.D. Mathur, J.F. Scott, Nature 442 (2006) 759.
[5] T. Zhao et al., Nat. Mater. 5 (2006) 823.
[6] J. Wu, Z. Shi, J. Xu, N. Li, Z. Zheng, H. Geng, Z. Xie, L. Zheng, Appl. Phys. Lett. 101 (2012) 122903.
[7] K.F. Wang, J.M. Liu, Z.F. Ren, Adv. Phys. 58 (2009) 321.
[8] C. Michel, J.-M. Moreau, G.D. Achenbache, R. Gerson, W.J. James, Solid State Commun. 7 (1969) 701.
[9] J.R. Teague, R. Gerson, W.J. James, Solid State Commun. 8 (1970) 1073.
[10] P. Fischer, M. Polomska, I. Sosnowska, M. Szymanski, J. Phys. C: Solid State Phys. 13 (1980) 1931.
[11] I. Sosnowska, T. Peterlin-Neumaier, E. Steichele, J. Phys. C: Solid State Phys. 15 (1982) 4835.
[12] G. Catalan, J.F. Scott, Adv. Mater. 21 (2009) 2463.
[13] T.-J. Park, G.C. Papaefthymiou, A.J. Viescas, A.R. Moodenbaugh, S.S. Wong, Nano Lett. 766 (2007).
[14] J. Wu, S. Mao, Z.-G. Ye, Z. Xie, L. Zheng, J. Mater. Chem. 20 (2010) 6512.
[15] N. Li, J. Wu, Y. Jiang, Z. Xie, L. Zheng, Z.-G. Ye, J. Appl. Phys. 113 (2013) 054102.
[16] W.M. Zhu, L.W. Su, Z.G. Ye, W. Ren, Appl. Phys. Lett. 94 (2009) 142908.
[17] Y.-J. Zhang, H.-G. Zhang, J.-H. Yin, H.-W. Zhang, J.-L. Chen, W.-Q. Wang, G.-H. Wu, J. Magn. Magn. Mater. 322 (2010) 2251.
[18] S.Y. Wang, X. Qiu, J. Gao, Y. Feng, W.N. Su, J.X. Zheng, D.S. Yu, D.J. Li, Appl. Phys. Lett. 98 (2011) 152902.
[19] V.A. Khomchenko, D.V. Karpinsky, A.L. Kholkin, N.A. Sobolev, G.N. Kakazei, J.P. Araujo, I.O. Troyanchuk, B.F.O. Costa, J.A. Paixa~o, J. Appl. Phys. 108 (2010) 074109.
[20] F. Azough, R. Freer, M. Thrall, R. Cernik, F. Tuna, D. Collison, J. Eur. Ceram. Soc. 30 (2010) 727.
[21] V.A. Khomchenko, I.O. Troyanchuk, M.I. Kovetskaya, J.A. Paixa~o, J. Appl. Phys. 111 (2012) 014110.
[22] A. Ianculescu, F.P. Gheorghiu, P. Postolache, O. Oprea, L. Mitoseriu, J. Alloys Comp. 504 (2010) 420.
[23] G. Kartopu, A. Lahmar, M. Es-Souni, Appl. Phys. Lett. 92 (2008) 151910.
[24] A. Lahmar, S. Habouti, C.-H. Solterbeck, M. Es-Souni, B. Elouadi, J. Appl. Phys. 105 (2009) 014111.
[25] C. Ederer, N.A. Spaldin, Phys. Rev. B 71 (2005) 060401.
[26] Y.-H. Lin, Q. Jiang, Y. Wang, C.-W. Nan, L. Chen, J. Yu, Appl. Phys. Lett. 90 (2007) 172501.
[27] M. Azuma, H. Kanda, A.A. Belik, Y. Shimakawa, M. Takano, J. Magn. Magn. Mater. 310 (2007) 1177.
[28] D.C. Arnold, K.S. Knight, F.D. Morrison, P. Lightfoot, Phys. Rev. Lett. 102 (2009) 027602.